





RESEARCH ARTICLE | FEBRUARY 24 2023

## Perturbed free induction decay obscures early time dynamics in two-dimensional electronic spectroscopy: The case of semiconductor nanocrystals

Special Collection: [Celebrating 25 Years of Two-dimensional Infrared \(2D IR\) Spectroscopy](#)

Patrick Brosseau ; H el ene Seiler ; Samuel Palato ; Colin Sonnichsen ; Harry Baker; Etienne Socie ; Dallas Strandell ; Patanjali Kambhampati  

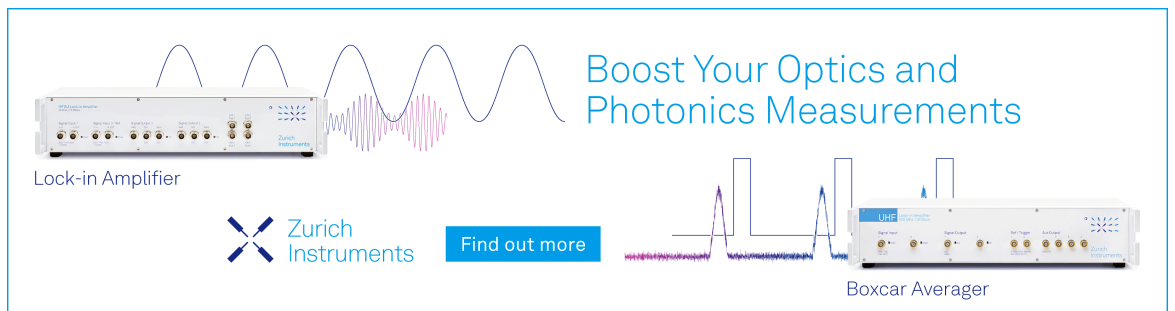


*J. Chem. Phys.* 158, 084201 (2023)

<https://doi.org/10.1063/5.0138252>




CrossMark



Boost Your Optics and Photonics Measurements

Lock-in Amplifier

 Zurich Instruments

[Find out more](#)

Boxcar Averager

# Perturbed free induction decay obscures early time dynamics in two-dimensional electronic spectroscopy: The case of semiconductor nanocrystals

Cite as: J. Chem. Phys. 158, 084201 (2023); doi: 10.1063/5.0138252

Submitted: 9 December 2022 • Accepted: 8 February 2023 •

Published Online: 24 February 2023



View Online



Export Citation



CrossMark

Patrick Brosseau,  H el ene Seiler,  Samuel Palato,  Colin Sonnichsen,  Harry Baker, Etienne Socie,   
Dallas Strandell,  and Patanjali Kambhampati<sup>a)</sup> 

## AFFILIATIONS

Department of Chemistry, McGill University, Montreal, Quebec H3A 0G4, Canada

**Note:** This paper is part of the JCP Special Topic on Celebrating 25 Years of Two-dimensional Infrared (2D IR) Spectroscopy.

<sup>a)</sup> Author to whom correspondence should be addressed: [pat.kambhampati@mcgill.ca](mailto:pat.kambhampati@mcgill.ca)

## ABSTRACT

Two-dimensional electronic spectroscopy (2DES) has recently been gaining popularity as an alternative to the more common transient absorption spectroscopy due to the combination of high frequency and time resolution of 2DES. In order to advance the reliable analysis of population dynamics and to optimize the time resolution of the method, one has to understand the numerous field matter interactions that take place at an early and negative time. These interactions have historically been discussed in one-dimensional spectroscopy as coherent artifacts and have been assigned to both resonant and non-resonant system responses during or before the pulse overlap. These coherent artifacts have also been described in 2DES but remain less well-understood due to the complexity of 2DES and the relative novelty of the method. Here, we present 2DES results in two model nanocrystal samples, CdSe and CsPbI<sub>3</sub>. We demonstrate non-resonant signals due to solvent response during the pulse overlap and resonant signals, which we assign to perturbed free induction decay (PFID), both before and during the pulse overlap. The simulations of the 2DES response functions at early and negative time delays reinforce the assignment of the negative time delay signals to PFID. Modeling reveals that the PFID signals will severely distort the initial picture of the resonant population dynamics. By including these effects in models of 2DES spectra, one is able to push forward the extraction of early time dynamics in 2DES.

Published under an exclusive license by AIP Publishing. <https://doi.org/10.1063/5.0138252>

## INTRODUCTION

Two-dimensional electronic spectroscopy (2DES) has proven to be a powerful method for studying coherent dynamics in electronic materials on an ultrafast timescale.<sup>1–6</sup> 2DES provides a combination of time and frequency resolution that is not possible with the more prevalent one-dimensional transient absorption (TA) spectroscopy, allowing 2DES to resolve correlational dynamics that are not accessible with TA spectroscopy, such as spectral ellipticity<sup>7,8</sup> and vibrational coherence maps.<sup>9–11</sup> However, modeling the signal during and before the pulse overlap is more complicated in 2DES as three or more pulses are used and multiple time delays are scanned, allowing for many pulse orderings in the same

experiment. The effective time resolution of 2DES is limited due to the complexity of resonant and non-resonant signals measured during the pulse overlap, and unlocking the full potential of the 2DES time resolution requires a thorough understanding of these signals.

In ultrafast nonlinear laser spectroscopy, two or more electric fields excite a sample and then a probe field triggers the emission of a signal field, or free induction decay (FID). Ultrafast experiments are generally designed with the intention that the excitation fields precede the probe field in time. However, when the probe and excitation fields overlap or the probe field precedes the excitation field, various unintended signals can be measured. These unintended signals are often termed “coherent artifacts,”<sup>12–16</sup> although this nomenclature

can be misleading as the term has been used to refer to a wide variety of phenomena and the term “coherent” can refer to coherent interaction between the laser fields or coherent interaction between the laser fields and the sample. Moreover, the coherent artifacts are not always truly artificial but are merely part of the material response to be understood.

Many of these unintended signals originate only when the excitation and probe fields are simultaneously present in the sample. For example, the simultaneous presence of both the excitation and probe pulses can instantaneously change the non-linear index of refraction of a material, resulting in non-resonant cross-phase modulation (XPM) of the probe field.<sup>17–19</sup> The coherent artifact can also be attributed to a transient thermal grating effect, where the excitation and probe fields spatially interfere and the excitation field is diffracted in the direction of the probe beam.<sup>14,15,20</sup> XPM and transient gratings need not originate from the sample itself and can originate from the cuvette or solvent. Therefore, these non-resonant signals can be identified in a solvent-only reference scan and can, in some cases, be removed.<sup>16,17</sup>

In addition to the non-resonant effects, the resonant sample response function measured during and before the pulse overlap can be particularly complex to interpret. The resonant coherent artifact effect was initially identified because the intensity of the coherent spike during the pulse overlap was observed to depend on the coherent dephasing time of the sample.<sup>12,13</sup> This resonant coherent effect can also extend before the pulse overlap, at negative time delays. Electric fields form coherent superpositions of states in a measured system, and these coherent states can dephase on a timescale longer than the pulse length. The interaction between the pump pulse and a long-lived FID at negative time delays can result in unintended signals being measured at negative time delays, before the pulses overlap. This phenomenon was widely noted in four-wave mixing (FWM) signals in semiconductor quantum wells at negative time delays several times longer than the pulse length due to the interaction between the excitation field and the long-lived dephasing of the exciton state.<sup>21–24</sup> This effect is also temperature dependent, as the coherence dephasing is slower at lower temperatures, meaning that reverse pulse ordering signals have more impact on cryogenic ultrafast spectroscopy.<sup>25</sup> This phenomenon has also been noted in two-pulse TA spectroscopy, under the name perturbed free induction decay (PFID). PFID in TA spectroscopy has been well discussed in the literature,<sup>22–24,26–32</sup> although this discussion is generally limited to near-infrared (NIR) and IR pump–probe experiments rather than those in the visible region. Due to the narrow linewidths seen in the IR regime, coherence dephasing often lasts longer than the pulse length, allowing for the resolution of the PFID at negative time delays. However, in room temperature visible TA, coherences often dephase within the pulse length and PFID is generally not resolved.

Several recent studies have noted that PFID signals appear at negative population times in 2DES and that this complicates the interpretation of dynamics near time zero.<sup>33–35</sup> Reversed pulse ordering signals have long been described in 2DIR<sup>36,37</sup> and 2D-THz spectroscopy<sup>38</sup> and have recently been discussed in detail in the 2DES literature.<sup>39,40</sup> Paleček *et al.* measured oscillating signals during and before the pulse overlap in 2DES, attributed to reversed pulse ordering double-sided Feynman diagrams (DSFDs) which can be misattributed to coherent superpositions of electronic or vibrational

states.<sup>39</sup> It is also shown that the pulse overlap region may extend much further than expected due to the long tails in the time profiles of the pulses.<sup>39</sup> Rose and Krich systematically generated the list of DSFDs that would theoretically occur for different pulse orderings in both third-order and fifth-order 2DES, and they calculated the corresponding fifth-order 2DES spectra.<sup>40</sup> These authors have opened the discussion of reversed pulse ordering signals in 2DES, although a full understanding of how these signals can affect various 2DES response functions requires detailed analysis for a variety of systems.

There are a number of model systems for 2DES, from photosynthetic reaction centers<sup>41–43</sup> to quantum wells<sup>44,45</sup> and nanocrystals (NCs).<sup>9,46,47</sup> In this work, we focus on NCs of two forms, previously studied by our group: CdSe quantum dot nanocrystals (QD-NCs)<sup>8,10,48–51</sup> and CsPbI<sub>3</sub> bulk perovskite NCs.<sup>8</sup> We immediately differentiate nanocrystals from quantum dots, as we have discussed in a recent review.<sup>52</sup> Both CdSe and CsPbI<sub>3</sub> represent model systems of the semiconductor NC form. In these materials, many processes occur in the first 100 fs, from charge carrier relaxation<sup>48,53</sup> to coherent phonon oscillations<sup>9,10</sup> and spectral diffusion.<sup>8</sup> An understanding of these early time dynamics requires the ability to push forward to as early a time as possible by understanding the early and negative time signals. Here, we explore both the resonant and non-resonant 2DES signals at population time delays from –100 to 200 fs. We model the 2DES response functions of both samples in this time range to demonstrate that PFID can obscure the determination of time-zero and the length of the instrument response function (IRF), and we show false line shape dynamics that could be misattributed to carrier relaxation or spectral diffusion.

## METHODS AND MATERIALS

The 2DES experiments were conducted on a previously described instrument.<sup>54</sup> In brief, the output of a Ti:sapphire amplifier (Coherent Legend Elite Duo HE+, 800 nm, 1 kHz, 130 fs) is broadened in a hollow core fiber (Few-cycle) filled with 3 atm of argon in a pressure gradient to generate a laser spectrum from 600 to 700 nm. The laser spectrum is temporally stretched in a grism pair before being split between two acousto-optic pulse shapers (Fastlite, Dazzler). The pulse shapers apply a phase mask to the spectrum to compress the pulse to ~15 fs, as confirmed by TG-FROG.

Three pulses are used in the experiment, labeled  $k_1$ ,  $k_2$ , and  $k_3$ . One of the pulse shapers diffracts the  $k_1$  and  $k_2$  pulses, separated by a time delay  $t_1$  and phase difference  $\phi$ , to be used as a pump beam. The other pulse shaper diffracts the final single pulse  $k_3$  to act as the probe. The pump beam crosses the sample at an angle and is stopped by a beam block, while the probe is transmitted straight through the sample and into a CCD spectrometer (Acton 2500i, PIXIS 100B Excelon). To measure a single 2DES spectrum, the time delay between the pump and probe pulses,  $t_2$ , is kept constant, while the time delay between the two pump pulses,  $t_1$ , is varied. A  $2 \times 2 \times 1$  phase cycling scheme is used, where the phase of the first two pulses is set to  $\phi = 0$  and  $\phi = \pi$  for each value of  $t_1$ . This phase cycling scheme allows for the simultaneous detection of the signals with  $k_1 - k_2 + k_3$  and  $-k_1 + k_2 + k_3$  wavevectors, corresponding to the non-rephasing and rephasing signals, respectively. A rotating frame is applied to the second pulse relative to the first pulse. The data are

Fourier transformed along  $t_1$  to generate a two-dimensional ( $E_1, E_3$ ) map. CdSe QD-NCs with a diameter of 6.9 nm were purchased from NNlabs, and CsPbI<sub>3</sub> NCs with an average edge size of 9.8 nm were synthesized using previously described methods.<sup>55,56</sup>

2DES spectra are simulated using standard methods,<sup>57</sup> as implemented in the Mbo.jl package (<https://github.com/spalato/Mbo.jl>). The third-order polarization, given by Eq. (1), is calculated as a sum of response functions,  $R_n(t_1, t_2, t_3)$ , convolved with the laser fields  $E_1, E_2$ , and  $E_3$ . The number of response functions at a specific set of time delays ( $t_1, t_2, t_3$ ) is equal to the number of possible DSFDs for the appropriate time ordering, as shown in Fig. S2,

$$P^{(3)}(t_1, t_2, t_3) \propto \int_0^\infty dt_3 \int_0^\infty dt_2 \int_0^\infty dt_1 \sum_n R_n(t_1, t_2, t_3) \times E_3(t-t_3)E_2(t-t_3-t_2)E_1(t-t_3-t_2-t_1). \quad (1)$$

For a given system, the set of response functions  $R_n$  are calculated with the same line shape function  $g(t)$  using the cumulant expansion truncated to second-order.<sup>57,58</sup> The 2DES spectra shown in Figs. 2, 3, 6(a), and 6(b) are simulated using<sup>57</sup> the Kubo line shape function

$$g^{Kubo}(t) = \Delta^2 \tau^2 \left( e^{-\frac{t}{\tau}} + \frac{-t}{\tau} - 1 \right), \quad (2)$$

where  $\Delta$  defines the width of the bath frequency fluctuations and  $\tau$  defines the timescale of the bath frequency fluctuation. The 2DES spectra shown in Figs. 5 and 6(c) are simulated using a vibrational line shape function<sup>57</sup>

$$g^{vib}(t) = S \left( \coth \left[ \frac{\hbar \omega_{vib}}{2k_B T} \right] [1 - \cos(\omega_{vib}t)] + i[\sin(\omega_{vib}t)] - \omega_{vib}t \right) + \gamma t + \sigma^2 t^2, \quad (3)$$

where  $S$  is the Huang–Rhys parameter,  $\omega_{vib}$  is the frequency of the vibrational mode,  $\gamma$  is the homogeneous broadening parameter, and  $\sigma$  is the inhomogeneous broadening parameter.

In a three-pulse 2DES experiment, where  $t_1$  is scanned at positive time delays and  $t_2$  is scanned at both negative and positive time delays, there are three pulse ordering regimes: [ $k_1, k_2, k_3$ ], [ $k_1, k_3, k_2$ ], and [ $k_3, k_1, k_2$ ]. Sixteen DSFDs, in total, are taken into account to calculate the 2DES line shape at different time delays.<sup>40</sup> At  $t_2 > 0$ , the line shape is calculated using the six DSFDs for the [ $k_1, k_2, k_3$ ] pulse ordering. At  $t_2 < 0$ , the line shape is calculated using the five DSFDs for the [ $k_3, k_1, k_2$ ] and [ $k_1, k_3, k_2$ ] pulse orderings, respectively. When all three pulses are overlapped, e.g., when  $t_1 = t_2 = 0$  fs, three more pulse orderings are possible: [ $k_3, k_2, k_1$ ], [ $k_2, k_1, k_3$ ], and [ $k_2, k_3, k_1$ ]. For simplicity, the signals originating from these last three pulse orderings are neglected in the calculations. Time delay  $t_1$  is incremented from 0 fs to 800 in steps of 2 fs, and time delay  $t_2$  is incremented from  $-400$  to 400 fs in steps of 2 fs. At  $t_2 < 0$ , the signal is multiplied by a phase factor of  $\phi = e^{i\omega_3 t_2}$  to take into account the time delay between the signal field and the local oscillator,  $k_3$ .<sup>36</sup>

## RESULTS

Figure 1 shows the 2DES spectra of the two model colloidal NC samples: CdSe QD-NCs and CsPbI<sub>3</sub> NCs. We have discussed the 2DES spectra of both systems in detail elsewhere.<sup>8,10,48–51</sup> The

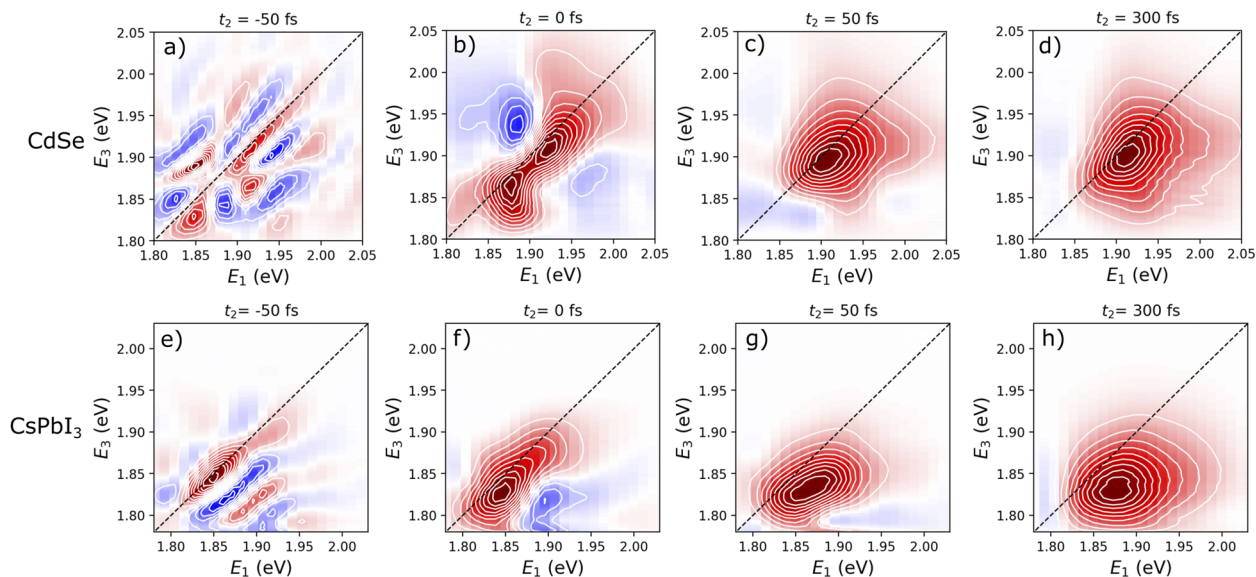


**FIG. 1.** Two-dimensional electronic spectroscopy (2DES) spectra at various population times,  $t_2$ , for [panels (a)–(d)] 6.9 nm CdSe quantum dot nanocrystals (QD-NCs) and [panels (e)–(h)] 9.8 nm CsPbI<sub>3</sub> perovskite nanocrystals (NCs). At  $t_2 = -50$  fs, narrow fringes parallel to the diagonal appear due to reversed pulse ordering. At  $t_2 = 0$  fs, when the pulses are fully overlapped, the 2DES spectra are still elongated along the diagonal. At  $t_2 = 300$  fs, the 2DES spectra broaden and broad positive and negative features appear due to bleaching, stimulated emission, or excited state absorption signals.

2DES spectra at four population times,  $t_2 = -50$  fs,  $t_2 = 0$  fs,  $t_2 = 50$  fs, and  $t_2 = 300$  fs, show qualitatively similar trends in both samples. At  $t_2 = -50$  fs, when pulse  $k_3$  arrives 50 fs before pulse  $k_2$ , both samples show narrow fringes parallel to the diagonal. At  $t_2 = 0$  fs, when pulses  $k_2$  and  $k_3$  are fully overlapped, the 2DES spectra are still elongated along the diagonal although the width along the anti-diagonal has broadened. By  $t_2 = 50$  fs, the pulses are well ordered as  $[k_1, k_2, k_3]$  and the 2DES spectra reveal broad spectral features that can be attributed to ground state bleach, stimulated emission, and excited state absorption pathways. From  $t_2 = 50$  to 300 fs, the line shape continues to evolve, reflecting the respective system–bath coupling of the two systems, as discussed previously.<sup>8</sup>

While 2DES data are generally presented as an energy–energy correlation plot,  $S(E_1, E_3)$ , as shown in Fig. 1, the reversed time-delay signals are best understood in the time domain. In the pump–probe beam geometry 2DES experiment, a single 2DES spectrum is collected in a mixed energy–time configuration,  $S(t_1, E_3)$ , where  $t_1$  is scanned and  $E_3$  is directly measured by a spectrometer. Figure 2 shows CsPbI<sub>3</sub> NC  $S(t_1, E_3)$  traces for four values of  $t_2$ : 200, -40, -60, and -80 fs. When  $t_2 = 200$  fs [Fig. 2(a)], an oscillating and decaying coherence signal is measured as a function of  $t_1$  and the wavefronts of the oscillating coherences are in phase along  $E_3$ . In the 2DES spectrum shown in Fig. 2(a), the signal is completely negative as the coherences are in phase along  $E_3$ . At  $t_2 = -40$  fs [Fig. 2(b)], an oscillating coherence is seen, but the amplitude of the coherence

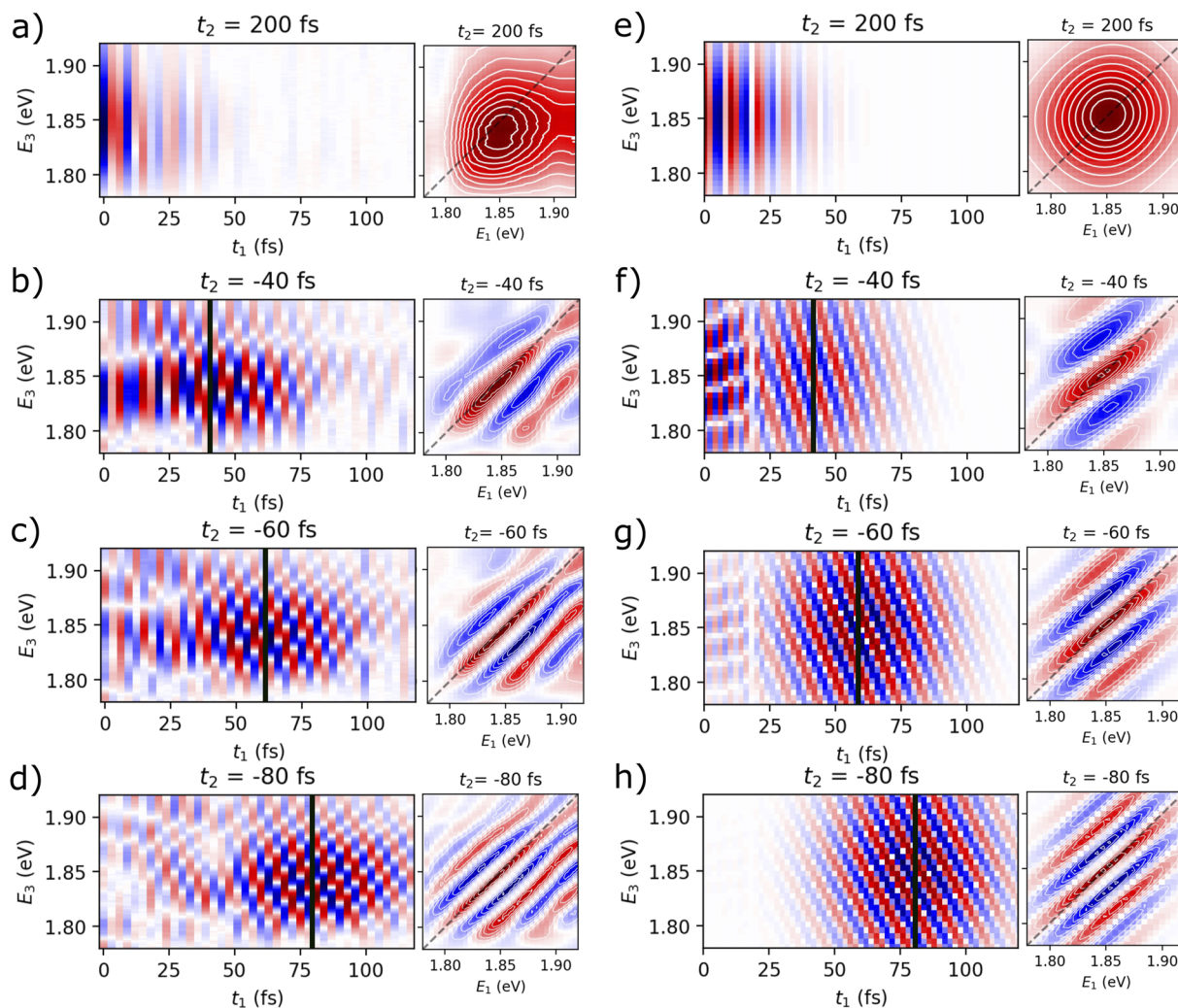


**FIG. 2.** Perturbed free-induction decay (PFID) in the energy–time domain and energy–energy domain for experimental CsPbI<sub>3</sub> 2DES (a)–(d) and a Kubo line shape simulation (e)–(h). At  $t_2 > 0$ , the coherence signal is given by the  $[k_1, k_2, k_3]$  pulse ordering, as shown in panels (a) and (e). When  $t_2 < 0$  and  $t_1$  is scanned, two different pulse orderings are sampled. The vertical black line in panels (b)–(d) and panels (f)–(h) shows the crossover between the  $[k_3, k_1, k_2]$  and  $[k_1, k_3, k_2]$  pulse orderings. The Fourier transform of the coherences results in fringes along the diagonal of the 2DES spectrum, as shown by the experimental spectra in panels (b)–(d) and reproduced by the simulations in panels (f)–(h).

risers and falls as a function of  $t_1$  and the wavefronts are slanted relative to  $E_3$ . In the 2DES spectrum shown in Fig. 2(b), both positive and negative spectral features are seen due to the shifting phase across the coherences. At  $t_2 = -60$  fs and  $t_2 = -80$  fs, the slanted coherences are still measured, but the peak of the coherence shifts to longer  $t_1$  values so that the peak of the oscillating coherence occurs around  $t_1 = |t_2|$ , marked by a vertical black line. This vertical black line also marks the transition from the  $[k_3, k_1, k_2]$  pulse ordering to the  $[k_1, k_3, k_2]$  pulse ordering. In all the 2DES spectra at  $t_2 < 0$  fs, diagonal fringes appear and the spacing of these fringes is inversely proportional to  $|t_2|$ .

The signals seen in the experimental traces shown in Figs. 2(a)–2(d) can be rationalized by simulating the response functions corresponding to the appropriate pulse ordering at every set of time delays ( $t_1, t_2$ ), as discussed above. Sixteen DSFDs, in total, are taken into account to calculate the line shape for the three pulse ordering regimes, as shown in Fig. S2. The series of quantum coherences that are generated in each of these three pulse ordering regimes are depicted in Fig. 3(c). At  $t_2 > 0$ , the line shape is calculated using the six DSFDs for the  $[k_1, k_2, k_3]$  pulse ordering. When  $t_2 < 0$  and  $|t_2| > t_1$ , the line shape is calculated using the five DSFDs for

the  $[k_3, k_1, k_2]$  pulse ordering. When  $t_2 < 0$  and  $|t_2| < t_1$ , the line shape is calculated using the five DSFDs for the  $[k_1, k_3, k_2]$  pulse ordering. When  $t_2 < 0$ , the coherence created by the first pulse interacting with the sample is cut short, so the effective coherence time is not  $t_1$  but  $t_{1,\text{eff}} = |t_2 - t_1|$ . Additionally, when the pulse ordering is reversed, a two-quantum coherence can be generated after a second pulse interacts with the sample. The effective two-quantum coherence time is  $t_{2,\text{eff}} = |t_2| - t_1$  with the  $[k_3, k_1, k_2]$  pulse ordering, and the effective two-quantum coherence time is  $t_{2,\text{eff}} = |t_2| + t_1$  with the  $[k_1, k_3, k_2]$  pulse ordering. As previously demonstrated for CsPbI<sub>3</sub> NCs,<sup>8</sup> the simulation in Figs. 2(a)–2(d) is given by a Kubo line shape function, as described above, with  $\Delta = 36$  meV and  $\tau = 85$  fs.

In addition to introducing new DSFDs and changing the effective coherence times, reversed pulse ordering changes the measured line shape by introducing a time delay between the emitted signal field,  $k_{\text{sig}}$ , and the local oscillator (LO),  $k_3$ . In ordinary 2DES pulse ordering in the pump–probe beam geometry,  $[k_1, k_2, k_3]$ , the emission of the signal field is triggered by  $k_3$  and, then,  $k_3$  also acts as the LO. If the pulse ordering is reversed,  $k_3$  still acts as the LO, but  $k_2$  triggers the emission of the signal field. Reverse pulse ordering

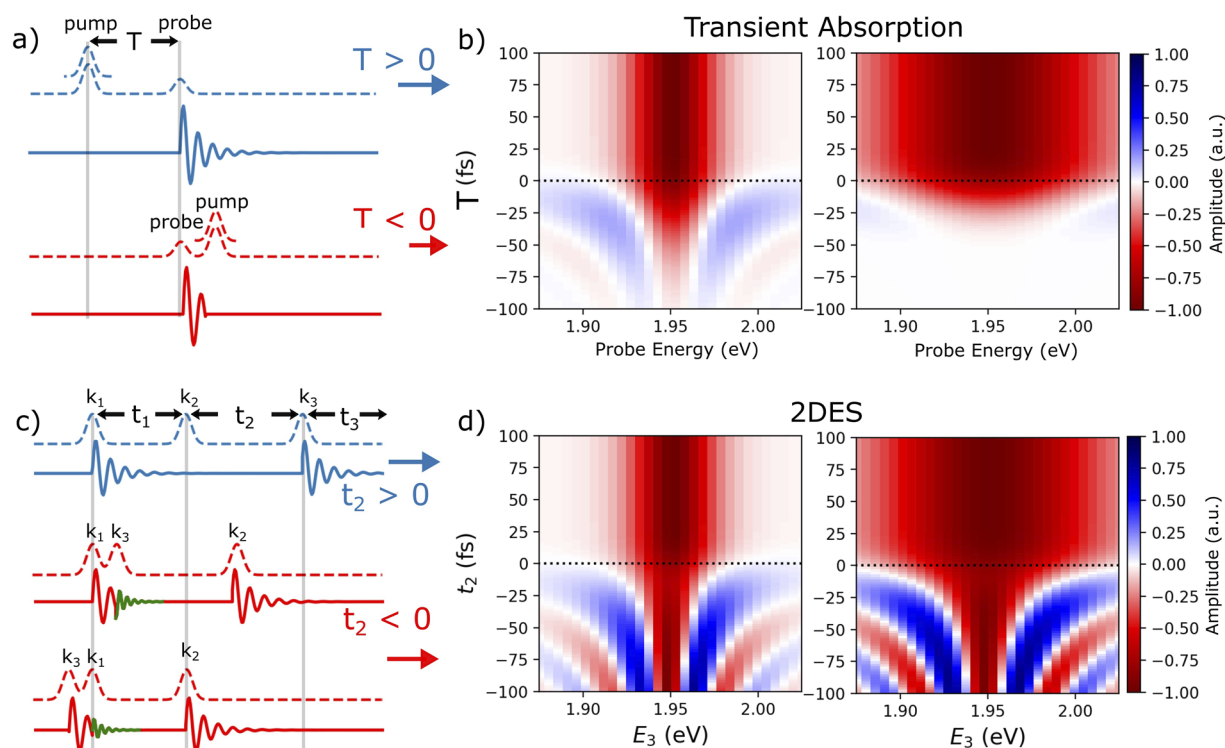


**FIG. 3.** Simulated PFID in transient absorption (TA) and 2DES experiments. (a) Pulse diagrams showing a TA experiment for the cases when the pump precedes the probe and when the pump follows the probe. In TA, the pump pulse interacts with the sample twice, shown by two concurrent pulses. (b) Simulated TA spectra for narrow (FWHM = 34 meV) and broad (FWHM = 92 meV) absorption linewidths. (c) Pulse diagrams showing a three-pulse 2DES experiment for difference pulse ordering cases. The blue diagram shows the case when  $t_2 > 0$  and the pulses are ordered as follows:  $[k_1, k_2, k_3]$ . The red diagrams show the cases when  $t_2 < 0$  and two other pulse ordering are possible:  $[k_1, k_3, k_2]$  and  $[k_3, k_1, k_2]$ . In the  $[k_1, k_2, k_3]$  case, as  $t_1$  is scanned, the measured signal oscillates due to the coherence between pulses  $k_1$  and  $k_2$ . In the reversed pulse order case, as  $t_1$  is scanned, multiple pulse orderings are sampled. (d) Pseudo-TA spectra extracted from the simulated 2DES spectra for a narrow and broad line shape, respectively. The pseudo-TA spectra correspond to excitation at  $E_1 = 1.95$  eV, as discussed in detail in the text.

creates a time delay between the signal and the LO fields, resulting in a phase difference between the two fields when they arrive at the detector.<sup>36,37</sup> The phase factor is given by  $\phi = e^{i(\frac{E_3}{\hbar} t_2)}$ , as the time delay between  $k_{\text{sig}}$  and the LO is  $t_2$  at  $t_2 < 0$ . The response functions shown in Figs. 2(f)–2(h) have been multiplied by the phase factor  $\phi$  to simulate the time delay between  $k_{\text{sig}}$  and the LO. This correlated phase generates the slanted wavefronts in the simulated coherences shown in Figs. 2(f)–2(h) and accounts for the slanted phase in the experimental coherences shown in Figs. 2(b)–2(d). In the  $(E_1, E_3)$  plots in Figs. 2(f)–2(h), the slanted fringes seen in the experimental spectra are recreated and the spacing of the simulated fringes is also inversely proportional to  $|t_2|$ . The direct correspondence between the experimental and simulated traces in Fig. 2 confirms that the signals seen at  $t_2 < 0$  in the 2DES experiments are due to resonant and correlated reversed pulse ordering signals.

The reversed pulse ordering signals in 2DES can be intuitively understood by comparing them to the more familiar case of PFID in a two-pulse TA experiment. Figure 3(a) depicts a TA experiment in the pump–probe and probe–pump pulse orderings. In the pump–probe ordering, the pump excites the system; then, the probe initiates the emission of the FID after a time delay  $T$ . In the probe–pump ordering, the probe generates FID and, then, the pump arrives later and perturbs this FID. Hence, the reversed pulse ordering signal in TA spectroscopy is generally referred to as perturbed free-induction decay, or PFID.<sup>29,30,59</sup> The PFID appears as spectral fringes in the TA spectrum at negative time delays, and the spacing of these fringes decreases as the pump–probe time delay becomes more negative.<sup>29,30,59</sup> The PFID has been measured in two-pulse TA experiments with narrow linewidths and long-lived FID, particularly in the near-IR<sup>29,30,59</sup> and IR<sup>26,28</sup> regions. PFID is generally not seen in visible TA experiments as the pulses used are long relative to the dephasing time of the FID. For example, the visible FID signal from an ensemble of CdSe QDs fully decays within 50 fs, while the time resolution of most TA experiments is greater than 100 fs. Hence, PFID is generally not considered when interpreting visible TA spectra, although PFID can be resolved with 10 fs pulses.<sup>60</sup>

Whether PFID is resolved in TA depends on the linewidth of the measured system. Figure 3(b) shows two simulated TA spectra. The TA spectra are generated by simulating the coherences for a 2DES spectrum with a Kubo line shape function at positive  $t_2$ . The negative time delay signal (PFID) is generated by setting the coherences to zero after the time delay  $t_1 = |t_2|$ , when  $t_2 < 0$ . The coherences are Fourier transformed to generate a 2DES spectrum, and a vertical slice of the 2DES spectrum is taken at  $E_1 = 1.95$  eV. In Fig. 3(b), on the left, a narrow line shape with  $\Delta = 20$  meV, a FWHM of 34 meV, and an FID lifetime of 90 fs is shown and, on the right, a broader line shape with  $\Delta = 50$  meV, a FWHM of 92 meV, and an FID lifetime of 35 fs is shown. A pulse length of 18 fs is used for both simulations, corresponding to a bandwidth of 200 meV. For the narrow linewidth, the PFID fringes can be clearly seen at  $T < 0$  fs, but for the broad linewidth, the PFID does not show distinctive fringes at  $T < 0$  fs. The PFID are only resolved in TA when the FID lifetime is significantly longer than the pulse length. This observation is consistent with the pump–probe experiments, which show that the PFID is stronger at cryogenic temperatures than at room temperature,<sup>31</sup> because, at low temperatures, the dephasing

lifetime of the FID increases and the PFID is easier to resolve. In samples with broad absorption features at room temperatures, such as semiconductor NCs, the visible TA spectra generally do not show PFID outside the pulse overlap region.<sup>61,62</sup>

As demonstrated in Figs. 1(a), 1(d), and 1(h), reversed pulse ordering signals can be measured in 2DES at  $t_2 = -50$  fs, significantly before  $t_2 = 0$  fs. These PFID signals can be resolved in 2DES experiments of nanocrystals despite fast electronic decoherence because the 2DES experiments used three pulses instead of two. The  $[k_1, k_2, k_3]$  pulse ordering is shown in the blue diagram in Fig. 3(c). The  $k_1$  pulse creates a coherence, the  $k_2$  pulse creates a population, then the  $k_3$  pulse once again creates a coherence, and the signal field  $k_{\text{sig}}$  is emitted. The red diagrams in Fig. 3(c) depict two cases of reversed pulse ordering:  $[k_1, k_3, k_2]$  and  $[k_3, k_1, k_2]$ . Even when the time delay between the  $k_2$  and  $k_3$  is large,  $k_1$  and  $k_3$  can still interact and generate a PFID signal at any negative time delay  $t_2$ .

Figure 3(d) shows two simulated pseudo-TA spectra extracted from the simulated 2DES spectra, with the same linewidths used in Fig. 3(b) and an 18 fs pulse. For the narrow linewidth, the FID lifetime is  $\sim 90$  fs and PFID can be clearly seen at  $t_2 < 0$  fs, as in the two-pulse TA case. For the broad linewidth, the FID lifetime is  $\sim 35$  fs. The FID does not last much longer than the pulse length, but the PFID can still be resolved at  $t_2 \ll 0$  fs due to the overlap of pulses  $k_1$  and  $k_3$  while scanning time delay  $t_1$ . While PFID can be justifiably ignored when interpreting room temperature visible TA data of samples with broad linewidths, PFID must be taken into account when interpreting any 2DES spectra.

Figure 2 shows that the spectral features at  $t_2 \ll 0$  fs in 2DES can be attributed to resonant reversed pulse ordering pathways and an accumulated phase factor that correlates the  $t_1$ ,  $t_2$ , and  $E_3$  axes. Near time-zero, however, the non-resonant solvent signals can also be measured in the 2DES spectra. Figure 4 shows the experimental 2DES results from CdSe NCs dispersed in toluene and from toluene alone. In Fig. 4(a), the transients correspond to a narrow integration area off the resonant CdSe absorption peak, as shown by the red circle in the inset. The CdSe response (solid line) and the solvent response (dotted line) are nearly identical, so at this energy, the measured 2DES signal can be primarily attributed to solvent response. The solvent signal has an oscillatory shape, is centered at  $t_2 = 0$  fs, lasts until  $t_2 = \sim 50$  fs, and can be attributed to an instantaneous process, such as XPM, during the pulse overlap.<sup>63</sup> In Fig. 4(b), the transients correspond to a narrow integration area centered at the resonant CdSe absorption peak, as shown by the blue circle in the inset. In this case, the CdSe response is much stronger than the solvent response, but an oscillatory signal can still be seen in the toluene transient near time-zero. After subtracting the solvent response from the CdSe transient, resulting in the dashed line, there remains a significant signal at  $t_2 \ll 0$  fs. We attribute the resonant CdSe signal at  $t_2 < 0$  fs to PFID. In Fig. 4(c), the transients correspond to a broad integration area centered at the resonant CdSe absorption peak, as shown by the green circle in the inset. In the broad integration case, the positive and negative fringes from PFID at  $t_2 < 0$  fs cancel out and the CdSe signal is close to zero at negative time delays. The 2DES signal before the pulse overlap is primarily due to PFID, while the signal during the pulse overlap is contaminated by both the PFID and non-resonant solvent contributions.

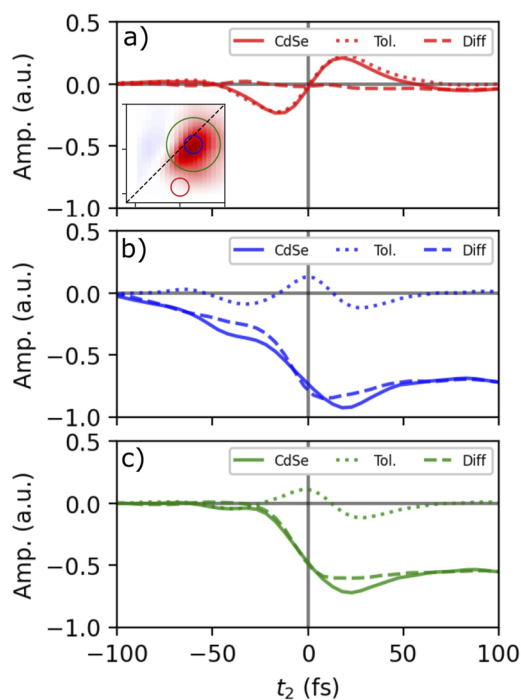


**FIG. 4.** Comparing the intensity of the resonant and non-resonant signals in CdSe NC 2DES. The solid lines show the response of CdSe NCs dispersed in toluene, while the dotted lines show the response of just toluene in a flow cell. The dashed lines correspond to the difference between the solid and dotted lines. The colored transients correspond to the integration areas in the inset in panel (a). (a) The red transients show the response where CdSe does not absorb strongly, (b) the blue transients show the response at the peak of the CdSe 2DES spectrum with a narrow integration width (20 meV), and (c) the green transients show the response at the peak of the CdSe 2DES spectrum with a broad integration width (60 meV).

It is possible to conduct a solvent reference scan and subtract non-resonant solvent contributions, such as XPM, although the PFID will persist as it originates from the resonant pathways in the sample itself. Many methods have been proposed for removing coherent artifact signals in various spectroscopies.<sup>12,16,27,28,64</sup> The methods for minimizing the PFID generally amount to smoothing out the narrow PFID fringes at  $t_2 \ll 0$ , as previously shown in the IR pump-probe.<sup>27,28,64</sup> In 2DES, the PFID at negative population times ( $t_2 \ll 0$ ) appears at late coherence times so that apodization will smooth out the PFID fringes at  $t_2 \ll 0$ , although the apodization would not significantly affect the PFID near  $t_2 = 0$  fs. As shown in Fig. 4(c), using a broad integration radius when extracting transients can remove the PFID fringes at  $t_2 \ll 0$ . In 2DES, such smoothing procedures are generally undesirable as maintaining a high frequency resolution is often the goal of the technique.<sup>9,63,66</sup> Coherent artifacts during the pulse overlap in 2DES have been shown to be polarization dependent,<sup>39</sup> so the variation of the pulse polarization could aid in minimizing these effects in 2DES.

Figure 5 shows the simulated 2DES spectra obtained using the vibrational line shape function in Eq. (3), where  $S = 0.25$ ,  $\omega_{vib} = 38$  rad/ps = 25 meV,  $\gamma = 25$  meV, and  $\sigma = 25$  meV. The 2DES simulations shown in Fig. 5(a) qualitatively recreate the

spectroscopic signatures of the PFID shown in Fig. 1 for CdSe NCs. At  $t_2 = -50$  fs, the PFID generates diagonal fringes; at  $t_2 = 0$  fs, the 2DES spectrum is elliptical; and from  $t_2 = 25$  to 200 fs, the 2DES spectrum features subtle line shape oscillations due to a coupling to the LO phonon.<sup>9,10</sup> Figure 5(b) tracks the transient intensity at three points labeled A, B, and C on the simulated 2DES spectra, with a 10 meV integration radius. Figure 5(c) shows the experimental transients in CdSe NCs, at the same three spectral positions, A, B, and C, with the solvent response subtracted. The experimental transients in Fig. 5(c) are qualitatively similar to the simulated transients in Fig. 5(b), and four effects of the PFID on the transient line shape dynamics are noted: (1) transients can be shifted toward negative  $t_2$ , obscuring time-zero; (2) transients can be shifted relative to each other, and this shift could be misattributed to population dynamics; (3) transients can be stretched toward negative  $t_2$ , obscuring the length of the IRF; and (4) positive signals can be generated that could be misattributed to excited state absorption or coherent oscillations. In aggregate, these four effects create a complicated spectral landscape during and before the pulse overlap in 2DES, although a qualitative understanding of these effects can help to disentangle the PFID contributions from the desired signals at positive delay times.

In TA spectroscopy, a transient can be modeled as a step function convolved with the IRF or, if modeling population dynamics, a step function and an exponential decay at positive time delays convolved with the IRF.<sup>62,67,68</sup> However, in 2DES, the PFID obscures both time-zero and the length of the IRF, so this simple fitting procedure would generally be ineffective. The PFID can also create the impression that the system dynamics are occurring on a timescale similar to the IRF. In both Figs. 5(a) and 5(b), the B transient is delayed relative to the A transient. The spectral response at point B vs point A could reflect hot carrier thermalization or spectral diffusion within a continuum of states, and the line shape transients associated with PFID can be mistaken for those dynamical processes. Furthermore, a positive signal is seen in transient C from  $t_2 = -30$  to 0 fs. Ordinarily, a positive feature could be attributed to an excited state absorption from a lower excited state to a higher excited state. However, the simulation in Fig. 5 only includes negative bleaching signals, so the positive signal in transient C in Fig. 5(b) must be attributed to a phase shift due to reverse pulse ordering. The early time-delay signals in 2DES introduce ambiguities that do not generally need to be considered in visible TA spectroscopy.

Figure 6(a) shows a 2DES simulation with the Kubo line shape function in Eq. (2), with  $\Delta = 36$  meV and  $\tau = 85$  fs and PFID at  $t_2 < 0$  fs. The 2DES simulations in Figs. 5(a) and 6(a) are qualitatively similar at  $t_2 = -50$  fs as the spectral line shape at negative  $t_2$  is primarily defined by the PFID rather than the resonant line shape. Figure 6(b) shows the FWHM of the anti-diagonal slice of the 2DES spectrum for the CsPbI<sub>3</sub> NCs (solid line) and the FWHM of the anti-diagonal of the simulated 2DES spectrum in Fig. 6(a) (dashed line). Both the experiment and the simulation follow the same trend, and the anti-diagonal broadens from  $t_2 = -100$  to 100 fs. In Fig. 6(b), the dotted line shows the same simulation without PFID at negative  $t_2$ , revealing that the broadening at negative time delays in the CsPbI<sub>3</sub> is due to PFID rather than a dynamical process in the NCs, such as spectral diffusion.<sup>8</sup> The anti-diagonal linewidth at  $t_2 = 0$  fs, ~50 meV, corresponds to the homogeneous linewidth of the CsPbI<sub>3</sub> NCs, and



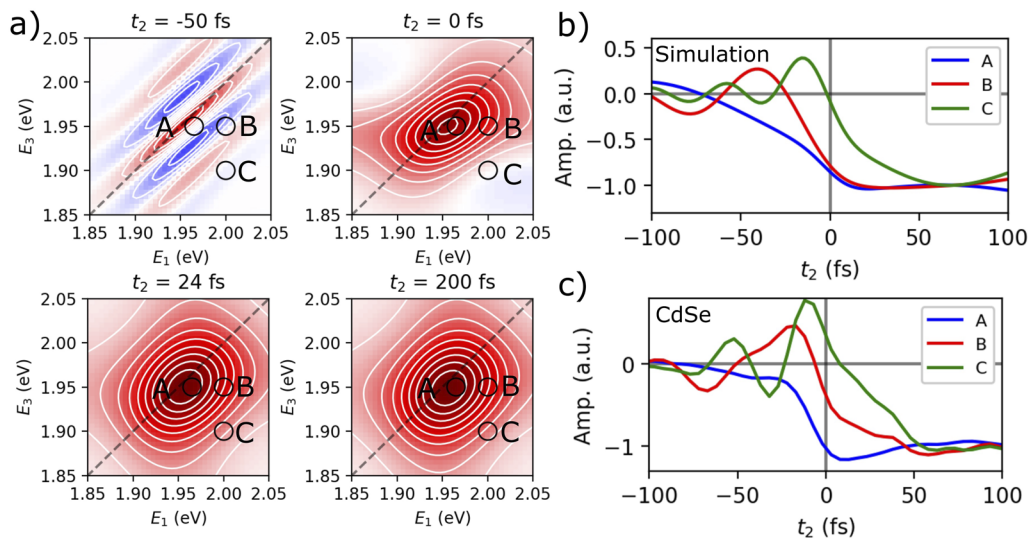


**FIG. 5.** Simulated 2DES spectra corresponding to the vibrational line shape function in Eq. (3), with  $S = 0.25$ ,  $\sigma = 25$  meV,  $\gamma = 25$  meV,  $\omega_{vib} = 38$  rad/ps, and an IRF of 25 fs. (a) 2DES spectra at various population times, showing diagonal fringes from PFID at  $t_2 = -50$  fs. (b) Transients for three different points in the simulated 2DES spectra, A, B, and C. (c) Transients for the points A, B, and C in CdSe NCs, extracted from the CdSe 2DES spectra in Fig. 1.

the narrower linewidth at negative delay time is unphysically narrow and distorted by the PFID.

Figure 6(c) shows the FWHM of the anti-diagonal slices of the 2DES spectrum for the CdSe NCs and a corresponding simulated 2DES trace obtained using the vibrational line shape function in Eq. (3). As in the CsPbI<sub>3</sub> NCs, the anti-diagonal becomes

unphysically narrow at negative time delays due to the PFID. Contrary to CsPbI<sub>3</sub> NCs, the anti-diagonal oscillates around a central value at  $t_2 > 0$  fs. This oscillation corresponds to exciton–phonon coupling with the CdSe LO phonon mode at  $\omega_{vib} = 38$  rad/ps = 25 meV.<sup>8</sup> Both CdSe and CsPbI<sub>3</sub> NCs reveal similar line shape dynamics during and before the pulse overlap region due to PFID,

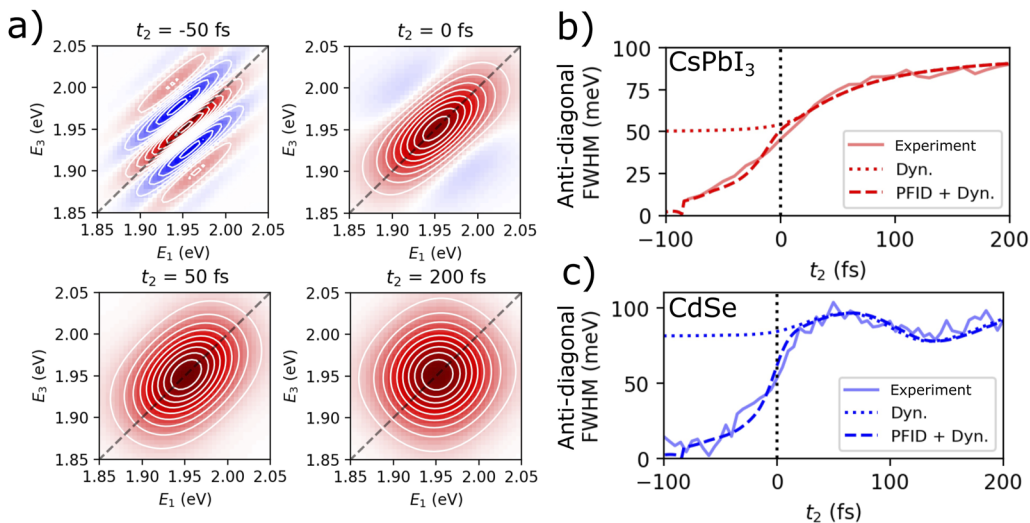


**FIG. 6.** Simulated 2DES spectra corresponding to the Kubo line shape function in Eq. (2) with  $\tau = 85$  fs,  $\Delta = 36$  meV, an IRF of 25 fs, and PFID at  $t_2 < 0$  fs. (a) 2DES spectra at various population times. (b) The FWHM of the anti-diagonal for the experimental CsPbI<sub>3</sub> 2DES spectra in Fig. 1 is shown with a solid line. The dashed line reflects the simulation in (a), showing broadening due to PFID at  $t_2 < 0$  and spectral diffusion at  $t_2 > 0$ . The dotted line shows the simulation without PFID, with no anti-diagonal dynamics at  $t_2 < 0$ . (c) The FWHM of the anti-diagonal for the experimental CdSe 2DES spectrum in Fig. 1 is shown with a solid line. The dashed line reflects the simulation in Fig. 5(a) showing broadening due to PFID at  $t_2 < 0$  and oscillations due to exciton–phonon coupling at  $t_2 > 0$ . The dotted line reflects the simulated 2DES spectrum without PFID, showing a flat line at  $t_2 < 0$ .

although, after  $t_2 = 25$  fs, the two samples reveal different line shape dynamics corresponding to their respective system–bath couplings.<sup>8</sup>

## CONCLUSIONS

Advances in coherent control and detection have significantly improved the quality of 2DES data in recent years and have made it possible to reliably resolve transient signals on short timescales. However, both resonant and non-resonant signals during and before the pulse overlap complicate the interpretation of the 2DES data in those regions. We have shown that, after the removal of the non-resonant solvent response, the PFID signals contaminate the early time transient data in 2DES measurements. These PFID signals have been demonstrated in two widely studied nanocrystal samples, CdSe and CsPbI<sub>3</sub>, showing a qualitatively consistent picture of PFID in both samples that originates from the experimental design and is independent of material composition. The agreement between the calculated and experimental 2DES spectra confirms that the PFID can obscure time-zero and the IRF length near the pulse overlap. The PFID can also introduce false excited state absorption and spectral diffusion signatures, as shown by spectral transients and anti-diagonal linewidths, respectively. These findings build upon the earlier work in the IR pump–probe and 2DIR and the recent work in 2DES, to establish a deeper understanding of the early time delay signals in visible TA and 2DES, providing a unified picture of the reversed pulse ordering signals in various ultrafast spectroscopies. A comparison between the simulated and experimental 2DES traces near time-zero can aid in confidently attributing the spectroscopic signatures to resonant physical processes in novel materials and avoiding the pitfalls of misleading spectroscopic signals.

## SUPPLEMENTARY MATERIAL

See the [supplementary material](#) for nanocrystal sample details, pulse characterization, and a detailed description of the simulation procedure.

## ACKNOWLEDGMENTS

We gratefully acknowledge the funding from the Canadian Foundation for Innovation (CFI), the Natural Sciences and Engineering Research Council of Canada (NSERC), Sony and McGill University. Samuel Palato thanks the NSERC for the financial support. H el ene Seiler thanks the Swiss National Science Foundation for the financial support.

## AUTHOR DECLARATIONS

### Conflict of Interest

The authors have no conflicts to disclose.

### Author Contributions

**Patrick Brosseau:** Conceptualization (lead); Data curation (lead); Formal analysis (lead); Writing – original draft (lead); Writing – review & editing (lead). **H el ene Seiler:** Conceptualization

(supporting); Data curation (supporting). **Samuel Palato:** Conceptualization (supporting); Data curation (supporting); Formal analysis (supporting). **Colin Sonnichsen:** Conceptualization (supporting); Data curation (supporting). **Harry Baker:** Data curation (supporting). **Etienne Socie:** Project administration (supporting); Resources (supporting). **Dallas Strandell:** Methodology (supporting); Project administration (supporting). **Patanjali Kambhampati:** Conceptualization (supporting); Funding acquisition (lead); Writing – original draft (supporting); Writing – review & editing (supporting).

## DATA AVAILABILITY

The data that support the findings of this study are available from the corresponding author upon reasonable request.

## REFERENCES

- 1 M. Maiuri, M. Garavelli, and G. Cerullo, “Ultrafast spectroscopy: State of the art and open challenges,” *J. Am. Chem. Soc.* **142**, 3–15 (2020).
- 2 E. Collini, “2D electronic spectroscopic techniques for quantum technology applications,” *J. Phys. Chem. C* **125**, 13096–13108 (2021).
- 3 A. Gelzinis, R. Augulis, V. Butkus, B. Robert, and L. Valkunas, “Two-dimensional spectroscopy for non-specialists,” *Biochim. Biophys. Acta, Bioenerg.* **1860**, 271–285 (2019).
- 4 S. Biswas, J. Kim, X. Zhang, and G. D. Scholes, “Coherent two-dimensional and broadband electronic spectroscopies,” *Chem. Rev.* **122**, 4257–4321 (2022).
- 5 C. L. Smallwood and S. T. Cundiff, “Multidimensional coherent spectroscopy of semiconductors,” *Laser Photonics Rev.* **12**, 1870052 (2018).
- 6 A. Liu, D. B. Almeida, L. A. Padilha, and S. T. Cundiff, “Perspective: Multidimensional coherent spectroscopy of perovskite nanocrystals,” *J. Phys.: Mater.* **5**, 021002 (2022).
- 7 P. J. Nowakowski, M. F. Khyasudeen, and H.-S. Tan, “The effect of laser pulse bandwidth on the measurement of the frequency fluctuation correlation functions in 2D electronic spectroscopy,” *Chem. Phys.* **515**, 214–220 (2018).
- 8 H. Seiler, S. Palato, C. Sonnichsen, H. Baker, E. Socie, D. P. Strandell, and P. Kambhampati, “Two-dimensional electronic spectroscopy reveals liquid-like lineshape dynamics in CsPbI<sub>3</sub> perovskite nanocrystals,” *Nat. Commun.* **10**, 4962 (2019).
- 9 T. A. Gellen, J. Lem, and D. B. Turner, “Probing homogeneous line broadening in CdSe nanocrystals using multidimensional electronic spectroscopy,” *Nano Lett.* **17**, 2809–2815 (2017).
- 10 S. Palato, H. Seiler, P. Nijjar, O. Prezhdo, and P. Kambhampati, “Atomic fluctuations in electronic materials revealed by dephasing,” *Proc. Natl. Acad. Sci. U. S. A.* **117**, 11940 (2020).
- 11 F. V. A. Camargo, H. L. Anderson, S. R. Meech, and I. A. Heisler, “Full characterization of vibrational coherence in a porphyrin chromophore by two-dimensional electronic spectroscopy,” *J. Phys. Chem. A* **119**, 95–101 (2015).
- 12 R. A. Engh, J. W. Petrich, and G. R. Fleming, “Removal of coherent coupling artifact in ground-state recovery experiments: Malachite green in water-methanol mixtures,” *J. Phys. Chem.* **89**, 618–621 (1985).
- 13 M. W. Balk and G. R. Fleming, “Dependence of the coherence spike on the material dephasing time in pump-probe experiments,” *J. Chem. Phys.* **83**, 4300–4307 (1985).
- 14 H. A. Ferwerda, J. Terpstra, and D. A. Wiersma, “Discussion of a ‘coherent artifact’ in four-wave mixing experiments,” *J. Chem. Phys.* **91**, 3296–3305 (1989).
- 15 M. V. Lebedev, O. V. Misochko, T. Dekorsy, and N. Georgiev, “On the nature of ‘coherent artifact,’” *J. Exp. Theor. Phys.* **100**, 272–282 (2005).
- 16 B. Dietzek, T. Pascher, V. Sundstr om, and A. Yartsev, “Appearance of coherent artifact signals in femtosecond transient absorption spectroscopy in dependence on detector design,” *Laser Phys. Lett.* **4**, 38–43 (2007).

- <sup>17</sup>A. Bresci, M. Guizzardi, C. M. Valensise, F. Marangi, F. Scotognella, G. Cerullo, and D. Polli, "Removal of cross-phase modulation artifacts in ultrafast pump-probe dynamics by deep learning," *APL Photonics* **6**, 076104 (2021).
- <sup>18</sup>K. Ekvall, P. Van Der Meulen, C. Dhollande, L.-E. Berg, S. Pommeret, R. Naskrecki, and J.-C. Mialocq, "Cross phase modulation artifact in liquid phase transient absorption spectroscopy," *J. Appl. Phys.* **87**, 2340–2352 (2000).
- <sup>19</sup>S. A. Kovalenko, A. L. Dobryakov, J. Ruthmann, and N. P. Ernstring, "Femtosecond spectroscopy of condensed phases with chirped supercontinuum probing," *Phys. Rev. A* **59**, 2369–2384 (1999).
- <sup>20</sup>T. F. Heinz, K. B. Eisenthal, and S. L. Palfrey, "Coherent coupling effects in pump-probe measurements with collinear, copropagating beams," *Opt. Lett.* **9**, 359 (1984).
- <sup>21</sup>D. S. Chemla and J. Shah, "Many-body and correlation effects in semiconductors," *Nature* **411**, 549–557 (2001).
- <sup>22</sup>K. Leo, E. O. Göbel, T. C. Damen, J. Shah, S. Schmitt-Rink, W. Schäfer, J. F. Müller, K. Köhler, and P. Ganser, "Subpicosecond four-wave mixing in GaAs/Al<sub>x</sub>Ga<sub>1-x</sub>As quantum wells," *Phys. Rev. B* **44**, 5726–5737 (1991).
- <sup>23</sup>K. Leo, M. Wegener, J. Shah, D. S. Chemla, E. O. Göbel, T. C. Damen, S. Schmitt-Rink, and W. Schäfer, "Effects of coherent polarization interactions on time-resolved degenerate four-wave mixing," *Phys. Rev. Lett.* **65**, 1340–1343 (1990).
- <sup>24</sup>M. Wegener, D. S. Chemla, S. Schmitt-Rink, and W. Schäfer, "Line shape of time-resolved four-wave mixing," *Phys. Rev. A* **42**, 5675–5684 (1990).
- <sup>25</sup>A. J. Fischer, D. S. Kim, J. Hays, W. Shan, J. J. Song, D. B. Eason, J. Ren, J. F. Schetzina, H. Luo, J. K. Furdyna, Z. Q. Zhu, T. Yao, J. F. Klem, and W. Schäfer, "Femtosecond coherent spectroscopy of bulk ZnSe and ZnCdSe/ZnSe quantum wells," *Phys. Rev. Lett.* **73**, 2368–2371 (1994).
- <sup>26</sup>P. Hamm, "Coherent effects in femtosecond infrared spectroscopy," *Chem. Phys.* **200**, 415–429 (1995).
- <sup>27</sup>P. Nuernberger, K. F. Lee, A. Bonvalet, T. Polack, M. H. Vos, A. Alexandrou, and M. Joffre, "Suppression of perturbed free-induction decay and noise in experimental ultrafast pump-probe data," *Opt. Lett.* **34**, 3226–3228 (2009).
- <sup>28</sup>S. Yan, M. T. Seidel, and H.-S. Tan, "Perturbed free induction decay in ultrafast mid-IR pump-probe spectroscopy," *Chem. Phys. Lett.* **517**, 36–40 (2011).
- <sup>29</sup>C. Wolpert, C. Dicken, L. Wang, P. Atkinson, A. Rastelli, O. G. Schmidt, H. Giessen, and M. Lippitz, "Ultrafast coherent spectroscopy of a single self-assembled quantum dot," *Phys. Status Solidi B* **249**, 721–730 (2012).
- <sup>30</sup>R. Mondal, B. Roy, B. Pal, and B. Bansal, "How pump-probe differential reflectivity at negative delay yields the perturbed-free-induction-decay: Theory of the experiment and its verification," *J. Phys: Condens. Matter* **30**, 505902 (2018).
- <sup>31</sup>M. H. Vos, J. Breton, and J.-L. Martin, "Electronic energy transfer within the hexamer cofactor system of bacterial reaction centers," *J. Phys. Chem. B* **101**, 9820–9832 (1997).
- <sup>32</sup>M. Joffre, C. B. à la Guillaume, N. Peyghambarian, M. Lindberg, D. Hulin, A. Migus, S. W. Koch, and A. Antonetti, "Coherent effects in pump-probe spectroscopy of excitons," *Opt. Lett.* **13**, 276 (1988).
- <sup>33</sup>J. M. Richter, F. Branchi, F. Valduga De Almeida Camargo, B. Zhao, R. H. Friend, G. Cerullo, and F. Deschler, "Ultrafast carrier thermalization in lead iodide perovskite probed with two-dimensional electronic spectroscopy," *Nat. Commun.* **8**, 376 (2017).
- <sup>34</sup>X. T. Nguyen, D. Timmer, Y. Rakita, D. Cahen, A. Steinhoff, F. Jahnke, C. Lienau, and A. De Sio, "Ultrafast charge carrier relaxation in inorganic halide perovskite single crystals probed by two-dimensional electronic spectroscopy," *J. Phys. Chem. Lett.* **10**, 5414–5421 (2019).
- <sup>35</sup>L. T. Lloyd, R. E. Wood, F. Mujid, S. Sohoni, K. L. Ji, P.-C. Ting, J. S. Higgins, J. Park, and G. S. Engel, "Sub-10 fs intervalley exciton coupling in monolayer MoS<sub>2</sub> revealed by helicity-resolved two-dimensional electronic spectroscopy," *ACS Nano* **15**, 10253–10263 (2021).
- <sup>36</sup>P. Hamm, M. Lim, W. F. DeGrado, and R. M. Hochstrasser, "Pump/probe self heterodyned 2D spectroscopy of vibrational transitions of a small globular peptide," *J. Chem. Phys.* **112**, 1907–1916 (2000).
- <sup>37</sup>K. M. Farrell and M. T. Zanni, "Phase stable, shot-to-shot measurement of third- and fifth-order two-quantum correlation spectra using a pulse shaper in the pump-probe geometry," *J. Chem. Phys.* **157**, 014203 (2022).
- <sup>38</sup>W. Kuehn, K. Reimann, M. Woerner, T. Elsaesser, and R. Hey, "Two-dimensional terahertz correlation spectra of electronic excitations in semiconductor quantum wells," *J. Phys. Chem. B* **115**, 5448–5455 (2011).
- <sup>39</sup>D. Paleček, P. Edlund, E. Gustavsson, S. Westenhoff, and D. Zigmantas, "Potential pitfalls of the early-time dynamics in two-dimensional electronic spectroscopy," *J. Chem. Phys.* **151**, 024201 (2019).
- <sup>40</sup>P. A. Rose and J. J. Krich, "Automatic Feynman diagram generation for nonlinear optical spectroscopies and application to fifth-order spectroscopy with pulse overlaps," *J. Chem. Phys.* **154**, 034109 (2021).
- <sup>41</sup>Y.-C. Cheng and G. R. Fleming, "Dynamics of light harvesting in photosynthesis," *Annu. Rev. Phys. Chem.* **60**, 241–262 (2009).
- <sup>42</sup>K. L. M. Lewis and J. P. Ogilvie, "Probing photosynthetic energy and charge transfer with two-dimensional electronic spectroscopy," *J. Phys. Chem. Lett.* **3**, 503–510 (2012).
- <sup>43</sup>J. Cao, R. J. Cogdell, D. F. Coker, H. G. Duan, J. Hauer, U. Kleinekathöfer, T. L. C. Jansen, T. Mančal, R. J. Dwayne Miller, J. P. Ogilvie, V. I. Prokhorenko, T. Renger, H. S. Tan, R. Tempelaar, M. Thorwart, E. Thyrraug, S. Westenhoff, and D. Zigmantas, "Quantum biology revisited," *Sci. Adv.* **6**, eaaz4888 (2020).
- <sup>44</sup>K. W. Stone, D. B. Turner, K. Gundogdu, S. T. Cundiff, and K. A. Nelson, "Exciton-exciton correlations revealed by two-quantum, two-dimensional Fourier transform optical spectroscopy," *Acc. Chem. Res.* **42**, 1452–1461 (2009).
- <sup>45</sup>D. B. Turner, P. Wen, D. H. Arias, K. A. Nelson, H. Li, G. Moody, M. E. Siemens, and S. T. Cundiff, "Persistent exciton-type many-body interactions in GaAs quantum wells measured using two-dimensional optical spectroscopy," *Phys. Rev. B* **85**, 201303(R) (2012).
- <sup>46</sup>D. B. Turner, Y. Hassan, and G. D. Scholes, "Exciton superposition states in CdSe nanocrystals measured using broadband two-dimensional electronic spectroscopy," *Nano Lett.* **12**, 880–886 (2012).
- <sup>47</sup>A. Liu, D. B. Almeida, W.-K. Bae, L. A. Padilha, and S. T. Cundiff, "Simultaneous existence of confined and delocalized vibrational modes in colloidal quantum dots," *J. Phys. Chem. Lett.* **10**, 6144–6150 (2019).
- <sup>48</sup>H. Seiler, S. Palato, and P. Kambhampati, "Investigating exciton structure and dynamics in colloidal CdSe quantum dots with two-dimensional electronic spectroscopy," *J. Chem. Phys.* **149**, 074702 (2018).
- <sup>49</sup>H. Seiler, S. Palato, C. Sonnichsen, H. Baker, and P. Kambhampati, "Seeing multiexcitons through sample inhomogeneity: Band-edge biexciton structure in CdSe nanocrystals revealed by two-dimensional electronic spectroscopy," *Nano Lett.* **18**, 2999–3006 (2018).
- <sup>50</sup>P. Brosseau, S. Palato, H. Seiler, H. Baker, and P. Kambhampati, "Fifth-order two-quantum absorptive two-dimensional electronic spectroscopy of CdSe quantum dots," *J. Chem. Phys.* **153**, 234703 (2020).
- <sup>51</sup>S. Palato, H. Seiler, H. Baker, C. Sonnichsen, P. Brosseau, and P. Kambhampati, "Investigating the electronic structure of confined multiexcitons with nonlinear spectroscopies," *J. Chem. Phys.* **152**, 104710 (2020).
- <sup>52</sup>P. Kambhampati, "Nanoparticles, nanocrystals, and quantum dots: What are the implications of size in colloidal nanoscale materials?," *J. Phys. Chem. Lett.* **12**, 4769–4779 (2021).
- <sup>53</sup>B. Yu, L. Chen, Z. Qu, C. Zhang, Z. Qin, X. Wang, and M. Xiao, "Size-dependent hot carrier dynamics in perovskite nanocrystals revealed by two-dimensional electronic spectroscopy," *J. Phys. Chem. Lett.* **12**, 238–244 (2021).
- <sup>54</sup>H. Seiler, S. Palato, B. E. Schmidt, and P. Kambhampati, "Simple fiber-based solution for coherent multidimensional spectroscopy in the visible regime," *Opt. Lett.* **42**, 643 (2017).
- <sup>55</sup>Q. Wang, X. Zheng, Y. Deng, J. Zhao, Z. Chen, and J. Huang, "Stabilizing the  $\alpha$ -phase of CsPbI<sub>3</sub> perovskite by sulfobetaine zwitterions in one-step spin-coating films," *Joule* **1**, 371–382 (2017).
- <sup>56</sup>L. Protesescu, S. Yakunin, M. I. Bodnarchuk, F. Krieg, R. Caputo, C. H. Hendon, R. X. Yang, A. Walsh, and M. V. Kovalenko, "Nanocrystals of cesium lead halide perovskites (CsPbX<sub>3</sub>, X = Cl, Br, and I): Novel optoelectronic materials showing bright emission with wide color gamut," *Nano Lett.* **15**, 3692–3696 (2015).
- <sup>57</sup>S. Mukamel, *Principles of Nonlinear Optical Spectroscopy* (Oxford University Press, 1995).
- <sup>58</sup>M. Cho, *Two-Dimensional Optical Spectroscopy* (CRC Press, 2009).
- <sup>59</sup>A. Rodek, T. Hahn, J. Kasprzak, T. Kazimierczuk, K. Nogajewski, K. E. Polczyńska, K. Watanabe, T. Taniguchi, T. Kuhn, P. Machnikowski, M. Potemski,

- D. Wigger, and P. Kossacki, “Local field effects in ultrafast light-matter interaction measured by pump-probe spectroscopy of monolayer MoSe<sub>2</sub>,” *Nanophotonics* **10**, 2717–2728 (2021).
- <sup>60</sup>J. Dana, O. S. Haggag, J. Dehnel, M. Mor, E. Lifshitz, and S. Ruhman, “Testing the fate of nascent holes in CdSe nanocrystals with sub-10 fs pump-probe spectroscopy,” *Nanoscale* **13**, 1982–1987 (2021).
- <sup>61</sup>S. L. Sewall, R. R. Cooney, E. A. Dias, P. Tyagi, and P. Kambhampati, “State-resolved observation in real time of the structural dynamics of multiexcitons in semiconductor nanocrystals,” *Phys. Rev. B* **84**, 235304 (2011).
- <sup>62</sup>G. Grimaldi, J. J. Geuchies, W. Van Der Stam, I. du Fossé, B. Brynjarsson, N. Kirkwood, S. Kinge, L. D. A. Siebbeles, and A. J. Houstepen, “Spectroscopic evidence for the contribution of holes to the bleach of Cd-chalcogenide quantum dots,” *Nano Lett.* **19**, 3002–3010 (2019).
- <sup>63</sup>K. Bouda, A. Fučíková, J. Pšenčík, and J. Alster, “Solvent signals in two-dimensional electronic spectroscopy,” *AIP Adv.* **12**, 115306 (2022).
- <sup>64</sup>T. Polack, “A filtering procedure for systematic removal of pump-perturbed polarization artifacts,” *Opt. Express* **14**, 5823 (2006).
- <sup>65</sup>F. V. A. De Camargo, L. Grimmelsmann, H. L. Anderson, S. R. Meech, and I. A. Heisler, “Resolving vibrational from electronic coherences in two-dimensional electronic spectroscopy: The role of the laser spectrum,” *Phys. Rev. Lett.* **118**, 033001 (2017).
- <sup>66</sup>E. Collini, H. Gattuso, L. Bolzonello, A. Casotto, A. Volpato, C. N. Dibenedetto, E. Fanizza, M. Striccoli, and F. Remacle, “Quantum phenomena in nanomaterials: Coherent superpositions of fine structure states in CdSe nanocrystals at room temperature,” *J. Phys. Chem. C* **123**, 31286–31293 (2019).
- <sup>67</sup>S. L. Sewall, R. R. Cooney, K. E. H. Anderson, E. A. Dias, and P. Kambhampati, “State-to-state exciton dynamics in semiconductor quantum dots,” *Phys. Rev. B* **74**, 235328 (2006).
- <sup>68</sup>S. L. Sewall, R. R. Cooney, K. E. H. Anderson, E. A. Dias, D. M. Sagar, and P. Kambhampati, “State-resolved studies of biexcitons and surface trapping dynamics in semiconductor quantum dots,” *J. Chem. Phys.* **129**, 084701 (2008).